Ground state of half-metallic zinc-blende MnAs

Stefano Sanvito* and Nicola A. Hill
Materials Department, University of California, Santa Barbara, California 93106
(Received 12 April 2000; revised manuscript received 17 July 2000)

In this paper we investigate theoretically the ground-state NiAs-type structure of MnAs and we compare the magnetic and structural properties with a hypothetical zinc-blende structure. A zinc-blende structure can be obtained, in principle, from the diluted magnetic semiconductor $Ga_{1-x}Mn_xAs$ in the limit $x=1$. Using density-functional calculations within the local spin-density approximation, we show that the zinc-blende structure, although showing half metallic behavior that is very attractive for spintronics, cannot be stabilized at equilibrium. We perform a tight-binding analysis of the Mn-As bond in the tetrahedral coordination to investigate the nature of the bonding in diluted magnetic semiconductors.

I. INTRODUCTION

In the last few years there has been a growing interest in combining magnetotransport experiments based on the giant magnetoresistance (GMR) in metallic magnetic multilayers with semiconductor physics.[1] Semiconductors offer various advantages over metals such as a very long spin lifetime,[2] persistent spin coherence,[3] and compatibility with existing semiconductor processing technologies. These properties pave the way for using semiconductors as media for storing coherence and realizing elements for solid-state quantum computation.[4] The natural extension of GMR to semiconductors is in a hybrid spin valve where the magnetic elements are either magnetic metals or diluted magnetic semiconductors[5,6] and the nonmagnetic elements are ordinary semiconductors. In both cases it is essential to inject spins into the nonmagnetic semiconductors and this is a formidable challenge.

So far, spin injection into semiconductors from metallic contacts has been elusive[7] with GMR signals smaller than 1%.[8,9] In contrast, spin injection from diluted magnetic semiconductors has been more successful, and evidence of polarized currents either into III-V (Ref. 10) and II-VI (Ref. 11) semiconductors has been demonstrated. In both cases, the polarization is observed by optical techniques, which makes the integration of such systems in present semiconductor technology very difficult and all electronic systems would be more technologically desirable. Recently it has been suggested[12] that a spin valve with a conventional injector-detector geometry made by metallic contacts cannot present large signals at equilibrium due to the very different resistivities of the contacts and the semiconductor spacer. Much larger signals are predicted by using half-metallic contacts or diluted magnetic semiconductors.

From the point of view of the materials, the system formed by GaAs as a nonmagnetic semiconductor and by MnAs and $Ga_{1-x}Mn_xAs$, respectively, as magnetic metal and diluted magnetic semiconductors is the most promising for spintronics applications. For the metallic component in metal/semiconductor structures, MnAs presents several advantages over transition metals. MnAs grows epitaxially onto GaAs in the hexagonal NiAs-type structure. This structure is characteristic of all bulk MnX compounds with X =As, Sb, and Bi. High-quality all-epitaxial MnAs structures can be grown onto commonly used GaAs (Refs. 13–15) and Si.[16] For MnAs/GaAs the interfaces are thermodynamically stable since the materials share the As atoms and the growth process is completely compatible with existing III-V molecular-beam epitaxy (MBE) technology.

Another attractive prospective crystal structure for MnAs is the zinc-blende structure. Recent density-functional calculations[17] have shown that the latter, which can be obtained in principle in the limit of 100% doping from $Ga_xMn_{1-x}As$, is a half metal. This makes zinc-blende MnAs very promising for spintronics because it will allow the intrinsic difficulty of injecting spins into semiconductors to be overcome.[12] Unfortunately to our knowledge zinc-blende MnAs has never been successfully grown.

In this paper we investigate, by using density-functional calculations, the stability of the NiAs-type MnAs with respect to the hypothetical zinc-blende structure. In particular, we look for growth conditions (for example, strains from the growing substrate or volume compressions) that can enable the zinc-blende phase to be made. One of the main results of this analysis is that the zinc-blende structure cannot be stabilized either by lattice stretching or by compression. We also consider the magnetic properties of the NiAs-type MnAs grown onto GaAs with different crystalline orientations and lattice distortions. Finally, we look at the nature of the chemical bonding in zinc-blende MnAs. This is particularly important since the tetrahedral coordination of the Mn atoms is one of the key elements for understanding the properties of magnetic diluted III-V semiconductors.

The remainder of this paper is organized as follows. In the next sections, we will briefly discuss the calculation technique and provide some information regarding the lattice structures considered and their properties. Then we will move on to analyze the stability of the NiAs-type MnAs under compression and distortion of the unit cell. In Sec. V, we will consider the zinc-blende structure and we will compare its structural properties with the NiAs type. Finally, we will perform a fit onto a tight-binding model in order to analyze the details of the chemical bonding in zinc-blende MnAs.

II. COMPUTATIONAL DETAILS

We compute the electronic structure of MnAs with both NiAs-type and zinc-blende lattice structures using a plane-wave pseudopotential implementation of the density-functional theory[18] with the local spin-density approximation. The use of pseudopotentials for the study of magnetic systems, although not yet as popular as all-electron methods, is now well documented.[19] We use the optimized pseudopotentials developed by Rappe *et al.*[20] for our Mn pseudopotential, allowing us to use a small cutoff energy for the plane-wave expansion in the total energy calculation of the solid. This is achieved by minimizing the kinetic energy in the high Fourier components of the pseudo-wave-function. The reference configuration for our Mn is $4s^{0.75}4p^{0.25}3d^5$ with core radii of 2.0, 2.15, and 2.0 a.u. and we use the usual Kleinman-Bylander separable form with two projectors for each angular momentum.[21,22] For As, we use the standard Hamann-Schülter-Chiang pseudopotential[23] with one projector for each angular momentum. The pseudopotentials were tested by comparing the pseudoeigenvalues with those generated by all-electron calculations for several atomic and ionic configurations. We also checked the portability by calculating the equilibrium lattice constant of GaAs and the dependence of the magnetization on the unit cell volume of hypothetical fcc Mn. Both are in excellent agreement with all-electron calculations. Moreover, the Mn pseudopotentials has been successfully used in earlier studies of perovskite manganites.[19]

Total energy and band structure are calculated by using the code SPECTER.[24] This is a spin-polarized implementation of density-functional theory written in C, which originated from the program CASTEP 2.1.[25] The plane-wave cutoff is fixed to 870 eV ($\sim$63 Ry) and we use a simple electron density mixing scheme for convergence developed by Kerker[26] with variable Gaussian broadening between 0.8 and 10^{-4} eV. We use a $4\times4\times4$ Monkhorst-Pack grid for the zinc-blende structure and a $3\times3\times3$ for the NiAs-type structure. This leads, respectively, to 10 and 6 k points in the corresponding irreducible Brillouin zones. Stability of the results with respect to k-point sampling has been carefully checked and the present choice represents a good compromise between accuracy and computation time. We observe that by doubling the number of irreducible k points, the total energy changes typically by less than 20 meV. Therefore, we consider 20 meV as the limit of the accuracy of our calculation.

III. CRYSTAL STRUCTURES

The NiAs-type lattice structure is a hexagonal structure (space group $P6_3/mmc$) with four atoms in the primitive unit cell (see Fig. 1). It is the equilibrium lattice structure of the pnictides formed with Mn at room temperature. Bulk MnAs has lattice constants of $a=3.7$ Å and $c=5.7$ Å and is a ferromagnetic metal with a T_c of 318 K. Above T_c it undergoes a phase transition to a paramagnetic state involving also a structural change to the hexagonal MnP-type lattice structure (space group $Pnma$) with a 2% volume reduction.[27] A further structural phase transition back to the NiAs-type phase is observed at 398 K with the material remaining paramagnetic.

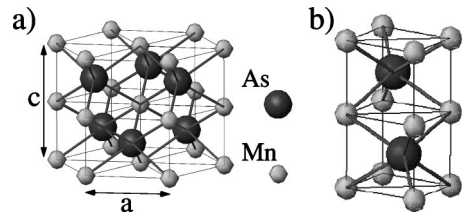

FIG. 1. (a) NiAs-type crystal structure. The lattice constants for bulk MnAs are $a=3.7$ Å and $c=5.7$ Å. (b) NiAs-type crystal structure: primitive cell.

MnAs can grow epitaxially onto GaAs in several possible crystalline orientations with respect to the GaAs substrate, depending on the growth conditions. In particular, when MnAs grows onto (001) GaAs, two orientations can occur.[28] The first one, which is usually called type *A*, has growth plane $(\bar{1}100)$ and epitaxial relationship $[\bar{1}\bar{1}20]$MnAs$\|[110]$GaAs and $[0001]$MnAs$\|[\bar{1}\bar{1}0]$GaAs, while the second, known as type *B*, has growth planes $(\bar{1}\bar{1}01)$ and $(\bar{1}\bar{1}02)$ and epitaxial relationship $[\bar{1}\bar{1}20]$MnAs$\|[\bar{1}\bar{1}0]$GaAs and $[1\bar{1}\bar{2}0]$MnAs$\|[110]$GaAs. Moreover, MnAs can be grown onto (111) GaAs (Ref. 29) with growth direction along the c axis of the hexagonal cell and epitaxial relationship (0001)MnAs$\|(111)$GaAs, $[\bar{1}100]$MnAs$\|[11\bar{2}]$GaAs, and $[\bar{2}110]$MnAs$\|[1\bar{1}0]$GaAs. All these phases have the easy axis of magnetization along the c axis of the hexagonal cell. The saturation magnetizations (M_s) are very different, being 416 emu/cm^3, 331 emu/cm^3,[28] and 640 emu/cm^3,[29] respectively, for type *A*, type *B*, and (111) GaAs grown MnAs. Moreover for MnAs MBE deposited onto GaAs, the saturation magnetization depends on the number of monolayers deposited,[30] suggesting that relaxation of the lattice has an important influence on the magnetic properties. In what follows, we will show that these changes of the saturation magnetization can be correlated with distortions of the hexagonal unit cell resulting from matching to the substrate.

Bulk zinc-blende MnAs is unstable, and zinc-blende structure thin films have not been demonstrated conclusively.[31] However, Mn can be incorporated into epitaxial layers of GaAs with concentrations beyond its solubility limit by using low temperature MBE techniques.[5] The highest concentration obtained so far is $x=0.07$ for $Ga_{1-x}Mn_xAs$, above which the Mn atoms segregate forming clusters of MnAs with NiAs-type structure. Nevertheless, the low-concentration limit is reproducible. Mn in GaAs acts both as a source of localized spin and also as an acceptor, providing electrical carriers (holes). (Ga,Mn)As is ferromagnetic for concentration above $x=0.005$, although the origin of the ferromagnetism is still a matter of debate. In Sec. V we will study the limit of $x=1$ in order to understand the nature of the chemical bond of Mn tetrahedrally coordinated with As.

IV. NiAs-TYPE MnAs

In this section we look at the magnetic properties and structural stability of the NiAs-type phase. In Fig. 2 we present the band structure for ferromagnetic MnAs with lattice parameter corresponding to the experimental bulk values

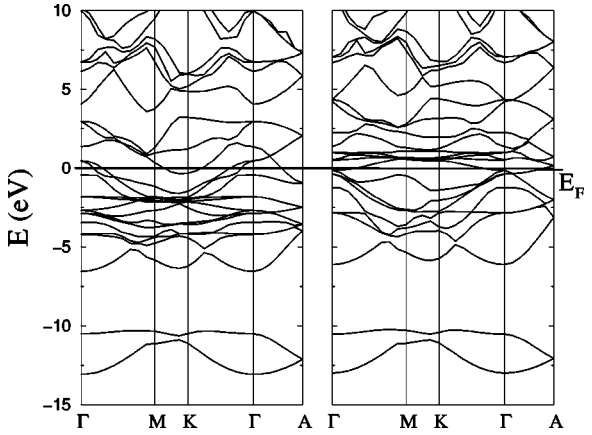

FIG. 2. Band structure for bulk MnAs with NiAs-type lattice structure. The figure on the left corresponds to the majority spin and the one to the right to the minority. The horizontal line denotes the position of the Fermi energy, which has been chosen to be 0 eV.

($a=3.7$ Å , $c=5.7$ Å). The two lower bands correspond to the $4s$ states of As, and the following 16 to hybridized p-d bands. This band structure is characteristic of all the Mn-based pnictides[27] and we can identify three distinct regions: (i) a low-energy p-d bonding region (between -6 and -2.5 eV for the majority band and between -6 and 0 eV for the minority), (ii) an almost dispersionless intermediate region (~ -2.0 for the majority and ~ 1 for the majority band) and (iii) a high-energy p-d antibonding region (between -1.5 and 3 eV for the majority band and between 1.5 and 4 eV for the minority). The ferromagnetism is mostly due to the spin splitting of the degenerate d bands, although a rigid shift model cannot be applied due to the strong p-d interaction. We will see in the next section that p-d interaction is also very strong in the zinc-blende structure.

Turning our attention to the structural properties we calculate the total energy and the magnetic moment per MnAs pair as a function of the volume occupied by a pair of atoms. We fix the ratio between the hexagonal axes to $c/a=1.54$, which corresponds to the experimental value for bulk MnAs. The results are presented in Fig. 3 (open squares).

Our calculated equilibrium volume is 31.123 Å ^{3} which is slightly smaller than the experimental one of 33.789 Å ^{3}. This small discrepancy can be explained by a general tendency of the local-density approximation (LDA) to underestimate the equilibrium volume. We also note that the structure is very stable with respect to compression and expansion of the unit cell around the equilibrium value (volume changes of the order of 50% give energy changes of approximately 1 eV). Our calculated magnetization M_s at equilibrium is between $2.5\mu_B$ and $3.0\mu_B$ which is smaller than that found experimentally ($\sim 3.4\mu_B$). Nevertheless, it is notable that the magnetization is very sensitive to the volume around the equilibrium position, and small volume changes can produce large changes in the magnetization. For large compressions the system evolves to a paramagnetic state. This transition is not directly comparable with experiments on MnAs under pressure[32] since a structural transition to the MnP-type structure and a magnetic transition to a mixed ferromagnetic and antiferromagnetic phase are experimentally observed for pressures above 4 kbar. In contrast, for volumes larger than

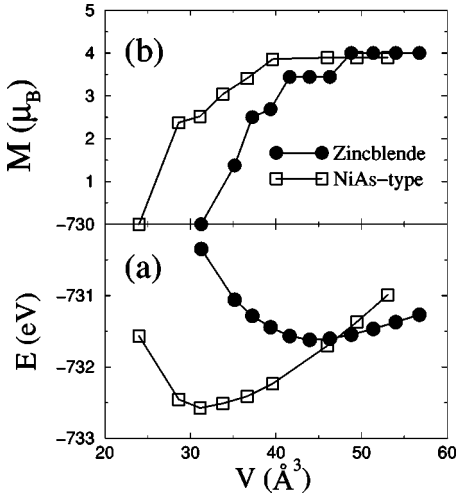

FIG. 3. Total energy (a) and magnetization (b) as a function of the MnAs pair volume for the NiAs-type (□) and the zinc-blende (●) structure. Note the large stability of the NiAs-type structure over a very broad volume range.

the equilibrium volume, we observe a saturation of the magnetic moment per MnAs pair to a value around $4\mu_B$. This saturation can be understood by comparing the band structures of Fig. 2 with those obtained for an expanded structure ($a=4.3$ Å $c=6.62$ Å with a volume per MnAs pair of 53.03 Å ^{3}) presented in Fig. 4. First we observe that there is a large shrinking of the Mn d bands without a drastic change of their centers with respect to the Fermi energy. As a result of the strong p-d interaction the minority p bands below the Fermi energy are pushed to higher energies, while the majority p bands above the Fermi energy are pulled to lower energy. This increases the number of occupied majority states and decreases the occupation of minority states resulting in a global increase in the magnetic moment of the system.

The saturation of the magnetization to a value of $\sim 4\mu_B$ can be explained by considering charge transfer from Mn to As. Three electrons will be transferred from each Mn to a neighboring As in order to fill completely the electronegative

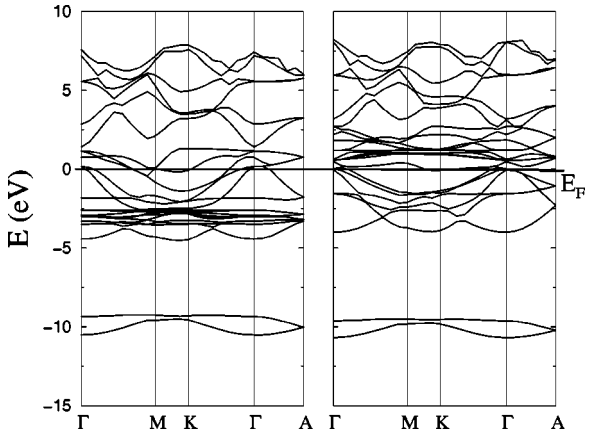

FIG. 4. Band structure of NiAs-type MnAs at expanded volume. The lattice constants are $a=4.3$ Å and $c=6.62$ Å . The figure on the left shows the majority spin and the one to the right the minority. The horizontal line denotes the position of the Fermi energy, which has been chosen to be 0 eV.

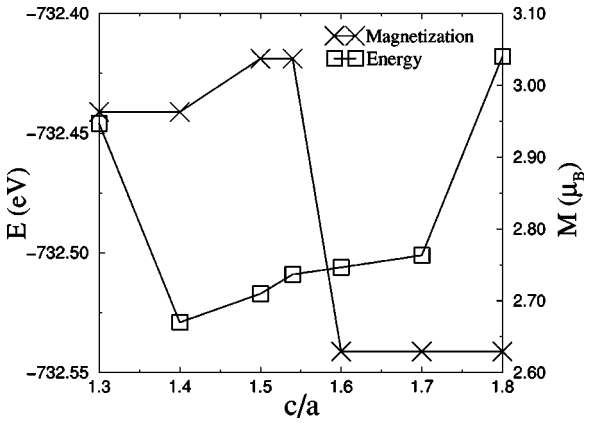

FIG. 5. Total energy (□ on the left-hand side scale) and magnetization (× on the right-hand side scale) as a function of the cell aspect ratio c/a. For bulk MnAs c/a=1.54.

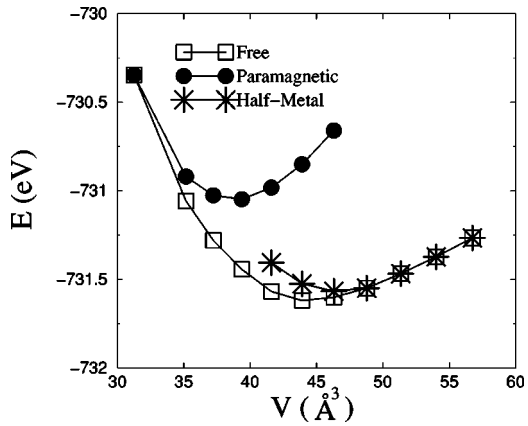

FIG. 6. Total energy as a function of the zinc-blende lattice spacing for the paramagnetic phase (●), the half-metallic phase (*), and for nonconstrained magnetic moment (□).

As atoms' $4p$ shell. This leads to an atomic configuration of Mn with four electrons in the valence, which arrange themselves following Hund's rules and produce a magnetic moment of $4\mu_B$. The charge transfer is not complete for unit cell volume corresponding to the experimental value because of the strong p-d interaction. This p-d interaction in fact leads also to a quite large negative polarization of the anions $(-0.23\pm0.05\mu_B)$, which has been observed with neutron scattering.[33] For stretched unit cells, the p-d hybridation is reduced and a more ionic configuration is resumed.

We finally look at the magnetization and the total energy of distorted cells. We consider cells with a volume equal to that of bulk MnAs and calculate the energy and the magnetization as a function of the cell aspect ratio c/a. Our results are presented in Fig. 5.

Several interesting aspects must be pointed out. First, note that the energy scale is much smaller than that of Fig. 3(a). The total energy for aspect ratios from 1.4 to 1.7 changes only by 25 meV (which is equal to k_BT at room temperature). This tiny variation is within the accuracy limit of the calculation and we can just conclude that for c/a going from 1.4 to 1.7, there is a large stability region. By comparing Figs. 3(a) and 5 one can conclude that NiAs-type MnAs can accommodate large distortions, which are much less energy demanding than volume changes. This can be easily understood by using a simple geometrical argument. Consider the nearest-neighbor distance $d_{\text{Mn-As}}$ as a function of the lattice constant a for fixed cell volume,

$$d_{\text{Mn-As}}=\frac{a}{\sqrt{3}}\sqrt{1+\frac{V_0^2}{a^6}}, \tag{1}$$

where V_0 is the volume occupied by a Mn-As pair. It is clear that $d_{\text{Mn-As}}$ is nonmonotonic with a minimum at $a=(2V_0)^{1/6}$, which is 3.629 Å in the case of bulk MnAs. Moreover, $d_{\text{Mn-As}}$ does not vary much with the lattice constant a around this minimum. For c/a increasing from 1.3 to 1.8, a increases by about 10% while $d_{\text{Mn-As}}$ increases by $\leqslant 1\%$. Since the total energy does not vary considerably as a function of the Mn-As bond angle, but only as a function of its bond length, we can conclude that the Mn-As bond is largely ionic and dominates the total energy. In fact, for the lattice distortions considered the second-nearest-neighbor distances (As-As and Mn-Mn) change drastically, while the first-nearest-neighbor distance (Mn-As) is almost constant. This produces no appreciable change in the total energy suggesting that the latter is dominated only by the Mn-As bond. Moreover, because of the absence of any strong angular dependence, we can also conclude that the Mn-As has a large ionic component.

Our calculated tiny energy variation for even large distortions, combined with the large change in magnetization at small distortions, explain most of the properties of the different epitaxial orientations of MnAs on GaAs. In fact it is worth noting that a large change of the magnetization occurs for ratios c/a just above the one corresponding to the bulk. The magnetization passes from a high-magnetization region $c/a<1.54$ to a low-magnetization region $c/a>1.54$. This is very important since large changes of the magnetization have been observed in MnAs grown onto GaAs with different crystalline orientations [type *A*, type *B*, and MnAs onto (111) GaAs]. It is difficult to correlate directly the deformation of the cell with the magnetization observed in experiments since a complicated surface reconstruction occurs[34] and a detailed characterization is not easy. We do not want to go into details of this intricate issue and we only suggest that the reduction of the magnetization of MnAs grown onto GaAs may be due to large deformation of the hexagonal lattice.

V. ZINC-BLENDE MnAs

We now consider MnAs with the zinc-blende lattice structure. In Fig. 6, we present the total energy as a function of the volume per formula unit for MnAs and also compare the total energy of the same structure when the magnetic moment is fixed either to $0\mu_B$ (paramagnetic phase) or to $4\mu_B$ (half-metallic phase). The equilibrium lattice constant is found between 5.6 Å ($V=43.904$ Å^3) and 5.7 Å ($V=46.298$ Å^3), which is very similar to the lattice constant of GaAs. Such a value is smaller (as we would expect within the LDA) than that predicted from the linear extrapolation of the experimental lattice constant of $Ga_{1-x}Mn_xAs$ for $x\rightarrow 1$ (5.89 Å).[5] It is also smaller than another LDA result obtained with the fully linear augmented plane wave (FLAPW) method (5.9 Å).[35] This could be due to the pseudopotential

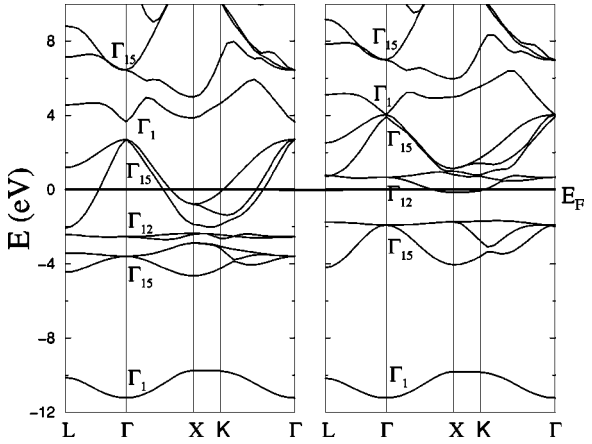

FIG. 7. Band structure for zinc-blende MnAs at the LDA energy minimum ($a=5.7$ Å). The figure on the left corresponds to the majority spin and the one on the right to the minority. The horizontal line denotes the position of the Fermi energy, which has been chosen to be 0 eV.

method used here or differences in convergence, or sampling between the two calculations. We do not fully understand the reason for such a disagreement. In order to shed some light on this point, we repeat the calculation with different pseudopotentials by using a density-functional code with pseudoatomic wave functions.[36] This leads to a similar equilibrium lattice constant that supports the present results. We also notice that the paramagnetic phase becomes energetically favorable for $a=5.0$ Å ($V=31.25$ Å^3), where a ferromagnetic to paramagnetic transition is predicted. In contrast, for lattice spacings larger than 5.8 Å ($V=48.778$ Å^3) a transition to an half metallic state is predicted. This is a very important result since half-metallicity is one of the conditions required to obtain large signals in a semiconductor spin valve.[12]

The behavior of the magnetization as a function of the unit cell volume is summarized in Fig. 3(b) (black circles). We notice that it looks similar to its counterpart for the NiAs-type structure (open squares) although in the latter, no transition to a half-metallic state is found. This fundamental difference between the two structures can be understood by looking at the band structure of zinc-blende MnAs in Fig. 7.

We first note that, excluding the presence of the Mn *d* bands, the band structure closely resembles that of the nonmagnetic III-V semiconductors. Consider the majority bands first. By symmetry analysis, we can easily identify the lower lying As *s* states (lowest band, Γ_1 at the Γ point), the As *p* valence band (first Γ_{15} point above E_F), and the first of the conduction bands (first Γ_1 point above E_F). However, due to the strong interaction with the Mn *d* states, the As *p* bands (top of the valence bands in GaAs) are pushed toward higher energies and become half filled. The Mn *d* bands, which are split into the doubly degenerate *e* band (Γ_{12}) and the triply degenerate t_2 band (Γ_{15}) are below the Fermi energy and entirely occupied. Therefore, one can conclude that two important interactions are present: (i) the *s*-*p* interaction giving rise to the sp^3 bond typical of nonmagnetic semiconductors and (ii) the *p*-*d* interaction responsible for the magnetism, which sets the position and the dispersion of the As *p* band. Note also that in contrast to the prediction from crystal field theory, the *e* orbitals possess higher energy than the t_2. This is also due to the strong *p*-*d* interaction. If we now turn our attention to the minority band, we can find most of the features of the majority. The main difference is the large split between the t_2 and the *e* states, which gives rise to a large gap in the band structure.

We observe that the Fermi energy cuts through the band center of the high-dispersion *p* band in the majority band, and through the band edge of the almost dispersionless *d* band in the minority. This is very important from the point of view of the transport, since very different spin-dependent effective masses are predicted. When the lattice constant is increased, we expect a general narrowing of all the bands. This does not affect qualitatively the majority band. However, for some critical lattice spacing, the band edge of the *e* band in the minority spin shifts above E_F giving rise to a semiconducting behavior. This generates the half metallicity.

In summary, if we start from the atomic configuration for Mn and As, the mechanism giving rise to the magnetism is the transfer of one electron from the Mn *d* orbitals to the As *p* shell in order to form the sp^3 bond. The remaining four electrons in the Mn *d* shell maximize the local magnetic moment of Mn due to Hund's coupling and the final state turns out to be ferromagnetic due to the strong *p*-*d* interaction. Note that these are features of the tetrahedral coordination and are absent in the NiAs-type structure, where no half metallic state is predicted.

Finally, we look at the stability of the zinc-blende structure with respect to the NiAs-type. The total energy and the saturation magnetization of both the structures as a function of the volume occupied by a MnAs pair are presented in Fig. 3(a). It is clear that the NiAs-type has a much lower total energy and also a more compressed lattice. Therefore, it is the stable structure at all the thermodynamically accessible pressures. This is consistent with the very small dilution limit of Mn in zinc-blende GaAs and with the fact that the annealing usually induces segregation of MnAs NiAs-type particles within the GaAs matrix.[5,6]

We also note that for very expanded unit cells, the zinc-blende structure becomes stable with a crossover volume that corresponds to a zinc-blende lattice constant of 5.8 Å. However, this large volume increase in the NiAs-type structure is very unlikely to occur, even if the lattice constants are forced to be large by growing onto substrates with large mismatch. As we noted previously, the NiAs-type structure can easily accommodate large cell distortions (Fig. 5). Therefore, at equilibrium it is energetically more favorable for the system to distort the cell, instead of increasing the volume and inducing a NiAs-type to zinc-blende transition.

Finally, we investigate the effect of the anion size on the stability properties of the zinc-blende structure. Our hope is that for larger ionic radii, the NiAs-type structure should become more rigid and a transition to the zinc-blende structure at large volume may be induced. We perform the same calculations described above for MnBi both with NiAs-type and zinc-blende structure (bulk MnBi is a ferromagnetic metal at room temperature with NiAs-type structure and lattice constants $a=4.17$ Å, $c=5.764$ Å). We did not find any relevant qualitative difference with respect to the MnAs case (see Fig. 8) and this is related to the geometrical argument presented in Sec. IV. Hence we conclude that, for all

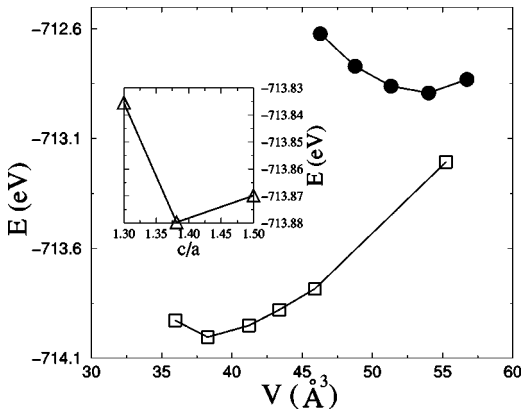

FIG. 8. Total energy as a function of the MnBi pair volume for the zinc-blende (●) and the NiAs-type structure (□). Note the large stability of the NiAs-type structure over a very broad volume range as in the MnAs case. In the inset, the energies for three different values of c/a for a volume corresponding to the bulk MnBi are shown. The central point corresponds to bulk MnBi ($V = 43.37$ Å^3).

the Mn-pnictides, the NiAs-type is the more stable crystalline structure and a transition to zinc-blende structure can be obtained only with highly nonequilibrium methods.

VI. Mn-As BOND IN THE ZINC-BLENDE STRUCTURE

Finally, to analyze the detailed nature of the Mn-As bonding in the zinc-blende lattice we perform a tight-binding fit to our calculated LDA band structure. We use a fitting algorithm included in the package OXON (Ref. 37) that minimizes the following function

$$f(E_n, \vec{\gamma}) = \sum_n \alpha_n |E_n(k) - E_n^c(k, \vec{\gamma})|, \qquad (2)$$

where $\vec{\gamma}$ is the m-dimensional vector containing the Slater-Koster tight-binding parameters,[38] α_n is the weight assigned to the eigenvalue E_n, and E_n^c is the computed eigenvalue. We consider first- (Mn-As) and second- (Mn-Mn and As-As) nearest-neighbor couplings. This interaction set has been shown to reproduce correctly the valence band and the first of the conduction bands of diamondlike semiconductors.[39] In the case of MnAs, the presence of the Mn d band makes the fitting procedure more complicated than in nonmagnetic semiconductors. However, we do not need to introduce any *ad hoc* excited state (such as s^*) to fit the valence band, and the first conduction band, as is frequently done in the literature.[40] The fit has been performed using 350 eigenvalues that correspond to the lowest 10 energies calculated at 35 k vectors and the weight is chosen to be one for each eigenvalue. We perform two independent fits for the majority and minority band allowing both the on-site energies and the hopping integrals to be different.

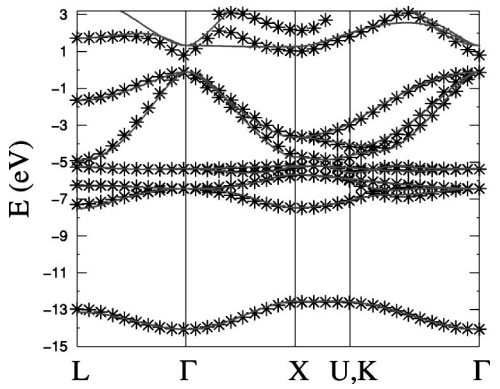

FIG. 9. Fit of the band structure for the majority band of MnAs. The stars (*) are the *ab initio* eigenvalues and the continuous line are the band calculated with the parameters of Tables I and II.

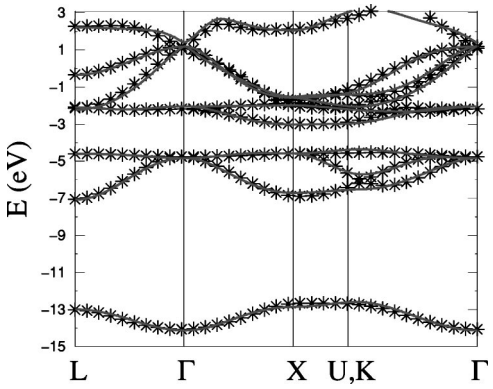

FIG. 10. Fit of the band structure for the minority band of MnAs. The stars (*) are the *ab initio* eigenvalues and the continuous line are the band calculated with the parameters of Tables I and II.

In Figs. 9 and 10 we present the best fits for the majority and minority spin band, respectively. We note that the agreement with the *ab initio* bands is remarkably good, in particular for the lower-lying bands. The highest bands are not well reproduced (in particular for the majority spin) because we did not include higher-energy bands in the fit. The complete parametrization giving rise to the bands in Figs. 9 and 10 is provided in Tables I and II.

Several important points must be stressed. First, we note that the major difference between the majority and the minority parameters is the value of the Mn $3d$ and As $4p$ on-site energies. The on-site energy of the $3d$ Mn orbitals coincides with the position of the e states, which by symmetry are weakly coupled to the other bands. By contrast, the t_2 states are strongly coupled to the above As p band and this coupling is strongly spin dependent. From Table II one can see that the dominant hopping integrals are along the Mn-As bond and that the parameters are quite similar for the two spin directions. The only parameters that differ strongly for

TABLE I. On-site energies for the majority and minority bands of zinc-blende MnAs. The notation is that of Slater and Koster (Ref. 38).

	Majority (eV)	Minority (eV)
$E_{\mathrm{As}(4s)}$	−9.8394	−9.9188
$E_{\mathrm{As}(4p)}$	−0.8709	−0.3476
$E_{\mathrm{Mn}(4s)}$	0.7380	−1.0519
$E_{\mathrm{Mn}(4p)}$	1.1254	1.4601
$E_{\mathrm{Mn}(3d)}$	−5.4699	−2.3417

TABLE II. Hopping integrals for the majority and minority bands of zinc-blende MnAs. The notation is that of Slater and Koster (Ref. 38).

	Majority (eV)	Minority (eV)
$E_{[\mathrm{As}(4s)-\mathrm{Mn}(4s)]\sigma}$	1.8554	1.3592
$E_{[\mathrm{As}(4s)-\mathrm{Mn}(4p)]\sigma}$	−1.8684	−1.5061
$E_{[\mathrm{As}(4s)-\mathrm{Mn}(3d)]\sigma}$	1.0852	2.0521
$E_{[\mathrm{As}(4p)-\mathrm{Mn}(4s)]\sigma}$	2.5898	2.3806
$E_{[\mathrm{As}(4p)-\mathrm{Mn}(4p)]\sigma}$	2.2825	2.5146
$E_{[\mathrm{As}(4p)-\mathrm{Mn}(4p)]\pi}$	−0.9342	−0.8346
$E_{[\mathrm{As}(4p)-\mathrm{Mn}(3d)]\sigma}$	1.0329	1.4592
$E_{[\mathrm{As}(4p)-\mathrm{Mn}(3d)]\pi}$	−0.4317	−0.6831
$E_{[\mathrm{As}(4s)-\mathrm{As}(4s)]\sigma}$	−0.0133	−0.1377
$E_{[\mathrm{As}(4s)-\mathrm{As}(4p)]\sigma}$	0.0031	0.0175
$E_{[\mathrm{As}(4p)-\mathrm{As}(4p)]\sigma}$	0.0009	0.0064
$E_{[\mathrm{As}(4p)-\mathrm{As}(4p)]\pi}$	0.0255	−0.0373
$E_{[\mathrm{Mn}(4s)-\mathrm{Mn}(4s)]\sigma}$	0.0000	0.0000
$E_{[\mathrm{Mn}(4s)-\mathrm{Mn}(4p)]\sigma}$	0.0053	−0.0009
$E_{[\mathrm{Mn}(4s)-\mathrm{Mn}(3d)]\sigma}$	−0.1579	0.1216
$E_{[\mathrm{Mn}(4p)-\mathrm{Mn}(4p)]\sigma}$	0.4411	0.3323
$E_{[\mathrm{Mn}(4p)-\mathrm{Mn}(4p)]\pi}$	−0.2265	−0.0167
$E_{[\mathrm{Mn}(4p)-\mathrm{Mn}(3d)]\sigma}$	0.2398	−0.2232
$E_{[\mathrm{Mn}(4p)-\mathrm{Mn}(3d)]\pi}$	−0.0298	0.1963
$E_{[\mathrm{Mn}(3d)-\mathrm{Mn}(3d)]\sigma}$	−0.1139	−0.1199
$E_{[\mathrm{Mn}(3d)-\mathrm{Mn}(3d)]\pi}$	0.0453	0.0773
$E_{[\mathrm{Mn}(3d)-\mathrm{Mn}(3d)]\delta}$	−0.0002	−0.0005

up and down spin are the $sd\sigma$, $pd\sigma$, and $pd\pi$ elements. These govern the repulsion of the t_2 Mn d bands and the As p bands and are responsible for the large e-t_2 splitting in the minority band.

Finally, we check our hypothesis on the formation of a strong sp^3 bond by comparing the ss, sp, and pp hopping integrals for MnAs with those of GaAs, which have been obtained with the same fitting procedure from our calculated LDA band structure. The GaAs parameters are shown in Table III and their magnitude is clearly comparable with the MnAs case. Moreover, the second-nearest-neighbor $pp\sigma$ and $pp\pi$ integrals, which are the only second-nearest-neighbor parameters with appreciable amplitude and the ones that describe most of the dispersion of the As p band along K $\rightarrow\Gamma$, are very similar. This clearly suggests the formation of a strong sp^3 bond in MnAs, together with a strong p-d hybridation.

VII. CONCLUSION

We have investigated theoretically the structural and magnetic properties of the hexagonal NiAs-type and the zinc-blende phases of MnAs. From the analysis, we conclude that the NiAs-type structure is more stable at all thermodynamic pressures. A phase transition to the zinc-blende structure is predicted for volume stretching, which in principle, could be obtained by growing onto a substrate with large lattice mismatch. However, the NiAs phase can accommodate large lattice distortions that preserve the Mn-As nearest-neighbor distance and a transition to a zinc-blende phase looks very unlikely.

TABLE III. Tight-binding parameters for GaAs. The notation is that of Slater and Koster (Ref. 38).

	GaAs (eV)
$E_{\mathrm{As}(4s)}$	−7.7859
$E_{\mathrm{As}(4p)}$	1.0395
$E_{\mathrm{Ga}(4s)}$	−0.2676
$E_{\mathrm{Ga}(4p)}$	2.8029
$E_{[\mathrm{As}(4s)-\mathrm{Ga}(4s)]\sigma}$	1.4895
$E_{[\mathrm{As}(4s)-\mathrm{Ga}(4p)]\sigma}$	−1.5445
$E_{[\mathrm{As}(4p)-\mathrm{Ga}(4s)]\sigma}$	2.5864
$E_{[\mathrm{As}(4p)-\mathrm{Ga}(4p)]\sigma}$	2.1571
$E_{[\mathrm{As}(4p)-\mathrm{Ga}(4p)]\pi}$	−0.7540
$E_{[\mathrm{As}(4s)-\mathrm{As}(4s)]\sigma}$	0.0032
$E_{[\mathrm{As}(4s)-\mathrm{As}(4p)]\sigma}$	−0.0437
$E_{[\mathrm{As}(4p)-\mathrm{As}(4p)]\sigma}$	−0.0009
$E_{[\mathrm{As}(4p)-\mathrm{As}(4p)]\pi}$	0.0010
$E_{[\mathrm{Ga}(4s)-\mathrm{Ga}(4s)]\sigma}$	−0.1038
$E_{[\mathrm{Ga}(4s)-\mathrm{Ga}(4p)]\sigma}$	−0.0919
$E_{[\mathrm{Ga}(4p)-\mathrm{Ga}(4p)]\sigma}$	0.4828
$E_{[\mathrm{Ga}(4p)-\mathrm{Ga}(4p)]\pi}$	−0.1512

We have also investigated the zinc-blende phase in more detail, since the tetrahedral coordination is crucial for the physics of diluted magnetic semiconductors. By performing both *ab initio* calculations and tight-binding fitting, we see that two important effects are present: (i) the formation of a stable sp^3 bond and (ii) a strong p-d hybridization, which splits the Mn d bands and gives rise to ferromagnetism. In particular for large lattice spacings, the zinc-blende structure is predicted to be half metallic.

ACKNOWLEDGMENTS

We would like to thank G. Theurich for having provided and supported the use of SPECTER and M. Fearn and A.P. Horsfield for the tight-binding package OXON. This work made use of MRL Central Facilities supported by the National Science Foundation under Award No. DMR96-32716. This work was supported by the DARPA/ONR under Grant No. N0014-99-1-1096, by ONR Grant No. N00014-00-10557, by NSF-DMR under Grant No. 9973076, and by ACS PRF under Grant No. 33851-G5. Useful discussions with N. Samarth, D.D. Awschalom, and L. Sham are kindly acknowledged.

*Email address: ssanvito@mrl.ucsb.edu

[1] G. Prinz, Phys. Today **48**, No. 4 (1995).
[2] J. M. Kikkawa and D. D. Awschalom, Phys. Rev. Lett. **80**, 4113 (1998).
[3] J. M. Kikkawa and D. D. Awschalom, Nature (London) **397**, 139 (1998).
[4] D. P. Di Vincenzo, Science **270**, 255 (1995).
[5] H. Ohno, J. Magn. Magn. Mater. **200**, 110 (1999).
[6] H. Ohno, Science **281**, 951 (1998).
[7] H. X. Tang, F. G. Monzon, R. Lifshitz, M. C. Cross, and M. L.

Roukes, Phys. Rev. B **61**, 4437 (2000), and references therein.
[8] W. Y. Lee, S. Gardelis, B. C. Choi, Y. B. Xu, C. G. Schmidt, C. H. W. Barnes, D. A. Ritchie, E. H. Linfield, and J. A. C. Bland, Appl. Phys. Lett. **85**, 6682 (1999).
[9] P. R. Hammer, B. R. Bennet, M. J. Yang, and M. Johnson, Phys. Rev. Lett. **83**, 203 (1999).
[10] Y. Ohno, D. K. Young, B. Beschoten, F. Matsukura, H. Ohno, and D. D. Awschalom, Nature (London) **402**, 790 (1999).
[11] R. Fiederling, M. Keim, G. Reuscher, W. Ossau, G. Schmidt, A. Waag, and L. W. Molenkamp, Nature (London) **402**, 787 (1999).
[12] G. Schmidt, L. W. Molenkamp, A. T. Filip, and B. J. van Wees, cond-mat/9911014 (unpublished).
[13] M. Tanaka, K. Saito, and T. Nishinaga, Appl. Phys. Lett. **74**, 64 (1999), and references therein.
[14] M. Tanaka, J. P. Harbison, T. Sands, B. Philips, T. L. Cheeks, J. De Boeck, F. T. Florez, and V. G. Keramidas, Appl. Phys. Lett. **63**, 696 (1993).
[15] M. Tanaka, J. P. Harbison, T. Sands, T. L. Cheeks, and V. G. Keramidas, J. Vac. Sci. Technol. B **12**, 1091 (1994).
[16] K. Akeura, M. Tanaka, M. Ueki, and T. Nishinaga, Appl. Phys. Lett. **67**, 3349 (1995).
[17] T. Ogawa, M. Shirai, N. Suzuki, and I. Kitagawa, J. Magn. Magn. Mater. **196-197**, 428 (1999).
[18] H. Hohenberg and W. Kohn, Phys. Rev. **136**, B864 (1964); W. Kohn and L. Sham, *ibid.* **140**, A1133 (1965).
[19] N. A. Hill and K. M. Rabe, Phys. Rev. B **59**, 8759 (1999).
[20] A. M. Rappe, K. M. Rabe, E. Kaxiras, and J. D. Ioannopolous, Phys. Rev. B **41**, 1227 (1990).
[21] L. Kleinman and D. M. Bylander, Phys. Rev. B **48**, 1425 (1982).
[22] P. E. Blöchl, Phys. Rev. B **41**, 5414 (1990).
[23] D. R. Hamann, M. Schülter, and C. Chiang, Phys. Rev. Lett. **43**, 1494 (1979).
[24] G. Theurich, B. Anson, N. A. Hill, and A. Hill, preprint submitted to Computing in Science and Engineering. The code is publically available at http://www.mrl.ucsb.edu/~theurich/Gespenst/ (unpublished).
[25] M. C. Payne, M. P. Teter, D. C. Allan, T. A. Arias, and J. D. Joannopoulos, Rev. Mod. Phys. **64**, 1045 (1992).
[26] G. P. Kerker, Phys. Rev. B **23**, 3082 (1981).
[27] K. Motizuki, K. Katoh, and A. Yanase, J. Phys. C **19**, 495 (1986), and references therein.
[28] M. Tanaka, J. P. Harbison, M. C. Park, Y. S. Park, T. Shin, and G. M. Rothberg, Appl. Phys. Lett. **65**, 1964 (1994).
[29] M. Tanaka, K. Saito, M. Goto, and T. Nishinaga, J. Magn. Magn. Mater. **198-199**, 719 (1999).
[30] M. Tanaka, J. P. Harbison, M. C. Park, Y. S. Park, T. Shin, and G. M. Rothberg, J. Appl. Phys. **76**, 6278 (1994).
[31] N. Samarth (private communication).
[32] K. Maki, T. Kaneko, H. Hiroyoshi, and K. Kamigaki, J. Magn. Magn. Mater. **177-181**, 1361 (1998).
[33] Y. Yamaguchi and H. Watanabe, J. Magn. Magn. Mater. **31-34**, 619 (1983).
[34] F. Schippan, A. Trampert, L. Däweritz, and K. H. Ploog, J. Vac. Sci. Technol. B **17**, 1716 (1999).
[35] M. Shirai, T. Ogawa, I. Kitagawa, and N. Suzuki, J. Magn. Magn. Mater. **177-181**, 1383 (1998).
[36] S. Sanvito, P. Ordejón, and N.A. Hill, preprint cond-mat/0011050.
[37] OXON [Oxford O(N) tight binding code] was developed at The Materials Modelling Laboratory of the Department of Materials at the University of Oxford.
[38] J. C. Slater and G. F. Koster, Phys. Rev. **94**, 1498 (1954).
[39] D. J. Chadi and M. L. Cohen, Phys. Status Solidi B **68**, 405 (1975).
[40] P. Vogl, H. P. Hjalmarson, and J. D. Dow, J. Phys. Chem. Solids **44**, 365 (1983).